TREND ANALYSIS OF FIXED PATTERN NOISE IN RAW IUE IMAGES

Joy Nichols-Bohlin
Computer Sciences Corporation
Astronomy Programs
Dec. 1, 1987

I. Introduction

The presence of fixed pattern noise in IUE data has been noted by numerous investigators over the past 10 years (see Appendix A for partial listing). The purpose of the present study is to determine if the fixed pattern noise (FPN) is constant in raw image space and if so, if it is constant over long periods of time. We will also attempt to explore the nature of the fixed pattern noise.

II. Analysis

Sixteen UV-flood images were chosen for the analysis to provide (1) time coverage over the lifetime of IUE, (2) 60% and 120% exposure levels, and (3) data from the SWP, LWP, and LWR cameras. The images selected are the same type of images used to construct the Intensity Transfer Functions (ITFs), and are listed in Table 1. The analysis was performed on a 256x256 pixel subimage of the raw image, centered at (512,308). This area of the image was chosen to avoid the center of the image, which is known to be noisier than other regions, and still to be entirely within the target ring. Also, this region is not saturated on the 120% exposures. A normalized "noise" image was generated by dividing the raw subimage with a 5x5 median-filtered version of itself. Hereafter, the "noise image" and "raw image" refer to this 256x256 pixel region.

Comparison of Individual Rows and Columns of Noise Image

From the noise images generated, selected lines and columns of the data were compared for early, middle and late images. Figure 1 contains two plots, one of row 150 of the noise image and one from column 150 of the noise image, comparing the data from LWR 1233 (early) and LWR 14533 (middle). Figure 2 represents the same row and column for LWR 1233 (early) and LWR 18067 (late). These are 60% exposure images. The plots in Figures 1 and 2 indicate that the noise patterns are repeated in the early, middle, and late noise images. The strong "absorption" feature in row 150 is a reseau mark and there seems to be

no movement in this feature over the time period examined. Peaks and valleys in the noise pattern correlate to a large degree in both the row and column directions. Figures 3 and 4 are similar to Figures 1 and 2, but represent the 120% exposure images from the LWR camera. Again, there is remarkable correlation between the the noise patterns of the early, middle, and late images, far more than would be expected from a random noise pattern.

Similar data for the LWP camera is presented in Figures 5 and 6. Because images (both flat-field and data) are scarce for the LWP camera prior to 1984, only a middle and a late image were chosen for comparison. Figure 5 compares the 60% exposure level images and Figure 6 compares the 120% exposure level images. The noise patterns again show a significant correlation between the two images. No reseau mark happens to fall in the row or column chosen in the case of the LWP camera.

Figures 7-10 contain the data for the SWP images chosen for analysis. Figure 7 is the comparison for row 150 and column 150 of the early and middle SWP 60% images. Figure 8 shows the same comparison for the early and late SWP 60% images. Figure 9 compares the early and middle SWP 120% images and Figure 10 compares the early and late SWP 120% images. In these four figures, the correlation between the noise patterns is much less marked than it was for the two long wavelength cameras.

The implication of this analysis is that the FPN is very nearly constant over the lifetime of the satellite for the two long-wavelength cameras, but is probably time-dependent for the SWP camera. The FPN could be spatially time-dependent,magnitude time-dependent, or both.

Cross-Correlation of Noise Images

To better understand the temporal behavior of the fixed pattern noise, a crude method of two-dimensional cross-correlating the noise images generated from each of the flat-field raw images was developed. One noise image was shifted by a few pixels in the row and/or column direction with respect to the second noise image. The first noise image was then subtracted from the second, and the mean and standard deviation about the mean calculated for the resulting differenced image. The same procedure was done with no shift between the images involved. Table 2 lists the image pairs tested, the exposure level of those images, and the standard deviation of the differenced images for shifts of (0,0),(+1,0),(+2,0),(0,+1), and (+3,+5).

An obvious minimum in the standard deviation in the case of a (0,0) shift would indicate that the FPN is constant for the period, while no clear minimum, or a clear minimum at one of the shifted positions, would indicate the magnitude or spatial orientation of the FPN is time-dependent. For the two long-wavelength cameras, a very clear minimum in the standard deviation of the differenced noise images is seen at a shift of (0,0). The other four shifts reported in this table have approximately equivalent standard deviations for each image. The standard deviation for the unshifted difference is an average of 64% of those for the shifted differences for the LWR and LWP images. The SWP camera shows a minimum also for the shift of (0,0), except for the early and late 120% level image comparison. However, the minimum standard deviation is not nearly as marked as in the LWP and LWR cameras.

The minimum is an average of 88% of the standard deviations for the shifted values. These results reinforce the conclusion reached above, that the FPN is constant with time in the LWP and LWR cameras but has a time-dependency in the SWP camera.

Comparison of Noise to DN Level of Data

To determine if the FPN is additive or multiplicative to the DN level of the image, the mean DN level of each raw image was compared to the standard deviation of the associated normalized noise image. Table 3 shows the mean DN and standard deviation of the noise image for each of the tested images. Figures 11 and 12 show plots of the mean DN level of each raw image vs. the standard deviation of the noise image for the LWP and LWR cameras. If the FPN is a fixed multiple of the DN level, we would expect the relation to be constant; in other words the line on the plot would be flat, showing a constant standard deviation of the noise for all DN levels. If the FPN is additive, then the plot should show a negative slope, which is the case.

Electronic Noise

In order to determine if electronic noise, generated during the read-out of the image, is present in IUE data, an average row was created of each of the normalized noise images. This average row was created by summing all of the rows in the normalized noise image and dividing by the number of rows. Any regular noise pattern in the rows (2-channel, 4-channel, 16-channel, etc.) should be enhanced in the average row. Figure 13 shows the comparison of the average noise row for SWP 1243 and SWP 28018. This plot indicates the possibility of a regular noise pattern every 4 pixels.

Fast Fourier Transforms were applied to each average row for each image analyzed. The magnitude of the power spectrum for some of these average rows are presented here. Figure 14 is the FFT of the average row of LWP 1470. Four-channel noise is clearly present. Figure 15 is the FFT of the average row of SWP 1243. Here, eight-channel noise is present, as well as four-channel noise. Figure 16, the FFT of SWP 28018, also shows eight-channel noise. Figure 17 is the FFT of LWR 18069. The four-channel noise pattern is again present, but there is quite a bit of low-level noise as well. However, while electronic noise is certainly present, it seems to be at a low level compared to the fixed pattern noise and random noise.

III. Conclusions and Recommendations

Although these results are preliminary and represent small statistics, several conclusions have been reached as the result of the investigations reported herein.

1. Fixed pattern noise appears to be constant in raw image space for the long wavelength cameras.
2. The magnitude of the fixed pattern noise is not a fixed multiple of the DN level; it is probably additive.

3. A distinct 4- and 8-channel noise pattern exists in SWP images, and a 4-channel noise pattern in the LWP and LWR data, but the pattern may not be constant in raw image space, or with time.

Based on the data presented here and the above conclusions, it seems feasible to attempt to remove the fixed pattern noise from raw images for the long wavelength cameras, because the fixed pattern noise appears constant with time for these cameras. If the fixed pattern noise is only spatially time-dependent (and not magnitude time-dependent), cross-correlation techniques should allow the ITF to be properly applied, thus reducing or eliminating the fixed pattern noise. This method may be applicable to the SWP camera data.

Table 1

IMAGE	LEVEL	DATE OF OBSERVATION
LWP 1468	60%	82031
LWP 3431	60%	84147
LWP 1470	120%	82031
LWP 3433	120%	84147
LWR 1233	60%	78084
LWR 14533	60%	82304
LWR 18067	60%	87090
LWR 1230	120%	78084
LWR 14535	120%	82304
LWR 18069	120%	87090
SWP 1252	60%	78085
SWP 18591	60%	82322
SWP 28016	60%	86084
SWP 1243	120%	78085
SWP 18590	120%	82322
SWP 28018	120%	86084

Table 2

Standard Deviations of the Differences
of Normalized Noise Images as One Image
Is Shifted With Respect to the Other

IMAGES DIFFERENCED	LEVEL	STANDARD DEVIATION				
		shift(0,0)	shift(+1,0)	shift(+2,0)	shift(0,+1)	shift(+3,+5)
LWP 1468 LWP 3431	60%	0.16261	0.27762	0.27738	0.29759	0.29664
LWP 1470 LWP 3433	120%	0.13920	0.22765	0.22629	0.23516	0.22664
LWR 1233 LWR 14533	60%	0.17553	0.21002	0.23057	0.23718	0.23115
LWR 1233 LWR 18067	60%	0.16050	0.24263	0.24497	0.25568	0.24329
LWR 1230 LWR 14535	120%	0.12513	0.17553	0.18217	0.18715	0.18104
LWR 1230 LWR 18069	120%	0.11314	0.19127	0.19186	0.19761	0.19027
SWP 1252 SWP 18591	60%	0.16167	0.19814	0.19697	0.20357	0.19596
SWP 1252 SWP 28016	60%	0.18765	0.21438	0.21371	0.21460	0.21400
SWP 1243 SWP 18590	120%	0.13787	0.15842	0.15828	0.15407	0.15879
SWP 1243 SWP 28018	120%	0.17939	0.16723	0.17210	0.17233	0.17152

Table 3

IMAGE	LEVEL	MEAN DN OF RAW IMAGE	ST DEV OF NOISE IMAGE
LWP 1468	60%	105.33	0.19412
LWP 3431	60%	99.375	0.19707
LWP 1470	120%	168.51	0.15662
LWP 3433	120%	158.76	0.16327
LWR 1233	60%	94.397	0.16399
LWR 14533	60%	94.948	0.16079
LWR 18067	60%	72.095	0.18009
LWR 1230	120%	161.62	0.12400
LWR 14535	120%	148.96	0.13272
LWR 18069	120%	116.18	0.14512
SWP 1252	60%	119.82	0.12509
SWP 18591	60%	82.911	0.15145
SWP 28016	60%	63.036	0.17323
SWP 1243	120%	191.40	0.09699
SWP 18590	120%	131.54	0.12542
SWP 28018	120%	103.89	0.14140

Figure Captions

Figure 1: A comparison of the noise patterns for a single row (top) and a single column (bottom) between an early LWR and a middle LWR 60% flat-field image. The top plot shows row 150 of the normalized noise image for LWR 1233 (solid line) and LWR 14533 (dotted line). The bottom plot shows column 150 of the normalized noise image for LWR 1233 (solid line) and LWR 14533 (dotted line).

Figure 2: A comparison of the noise patterns for a single row (top) and a single column (bottom) between an early LWR and a late LWR 60% flat-field image. The top plot shows row 150 of the normalized noise image for LWR 1233 (solid line) and LWR 18067 (dotted line). The bottom plot shows column 150 of the normalized noise image for LWR 1233 (solid line) and LWR 18067 (dotted line).

Figure 3: A comparison of the noise patterns for a single row (top) and a single column (bottom) between an early LWR and a middle LWR 120% flat-field image. The top plot shows row 150 of the normalized noise image for LWR 1230 (solid line) and LWR 14535 (dotted line). The bottom plot shows column 150 of the normalized noise image for LWR 1230 (solid line) and LWR 14535 (dotted line).

Figure 4: A comparison of the noise patterns for a single row (top) and a single column (bottom) between an early LWR and a late LWR 120% flat-field image. The top plot shows row 150 of the normalized noise image for LWR 1230 (solid line) and LWR 18069 (dotted line). The bottom plot shows column 150 of the normalized noise image for LWR 1230 (solid line) and LWR 18069 (dotted line).

Figure 5: A comparison of the noise patterns for a single row (top) and a single column (bottom) between an middle LWP and a late LWP 60% flat-field image. The top plot shows row 150 of the normalized noise image for LWP 1468 (solid line) and LWP 3431 (dotted line). The bottom plot shows column 150 of the normalized noise image for LWP 1468 (solid line) and LWP 3431 (dotted line).

Figure 6: A comparison of the noise patterns for a single row (top) and a single column (bottom) between an middle LWP and a late LWP 120% flat-field image. The top plot shows row 150 of the normalized noise image for LWP 1470 (solid line) and LWP 3433 (dotted line). The bottom plot shows column 150 of the normalized noise image for LWP 1470 (solid line) and LWP 3433 (dotted line).

Figure 7: A comparison of the noise patterns for a single row (top) and a single column (bottom) between an early SWP and a middle SWP 60% flat-field image. The top plot shows row 150 of the normalized noise image for SWP 1252 (solid line) and SWP 18591 (dotted line). The bottom plot shows column 150 of the normalized noise image for SWP 1252 (solid line) and SWP 18591 (dotted line).

Figure 8: A comparison of the noise patterns for a single row (top) and a single column (bottom) between an early SWP and a late SWP 60% flat-field image. The top plot shows row 150 of the normalized noise image for SWP 1252 (solid line) and SWP 28016 (dotted

line). The bottom plot shows column 150 of the normalized noise image for SWP 1252 (solid line) and SWP 28016 (dotted line).

Figure 9: A comparison of the noise patterns for a single row (top) and a single column (bottom) between an early SWP and a middle SWP 120% flat-field image. The top plot shows row 150 of the normalized noise image for SWP 1243 (solid line) and SWP 18590 (dotted line). The bottom plot shows column 150 of the normalized noise image for SWP 1243 (solid line) and SWP 18590 (dotted line).

Figure 10: A comparison of the noise patterns for a single row (top) and a single column (bottom) between an early SWP and a late SWP 120% flat-field image. The top plot shows row 150 of the normalized noise image for SWP 1243 (solid line) and SWP 28018 (dotted line). The bottom plot shows column 150 of the normalized noise image for SWP 1243 (solid line) and SWP 28018 (dotted line).

Figure 11: Plot of mean DN level of the LWR raw images vs. standard deviations of the associated normalized noise images.

Figure 12: Plot of mean DN level of the LWP raw images vs. standard deviations of the associated normalized noise images.

Figure 13: A comparison of the noise patterns in the average rows of SWP 1243 and SWP 28018.

Figure 14: Plot of FFT of the average row of LWP 1470. Note the 4-channel noise pattern.

Figure 15: Plot of FFT of the average row of SWP 1243. Note the 4- and 8-channel noise patterns.

Figure 16: Plot of FFT of the average row of SWP 28018. Note the 4- and 8-channel noise patterns.

Figure 17: Plot of FFT of the average row of LWR 18069. A significant amount of low level noise is present, although the 4-channel noise is seen.

```
IUE_IDL>;line 150
IUE_IDL>;solid line:  LWR 1233   dotted line: LWR 14533
```

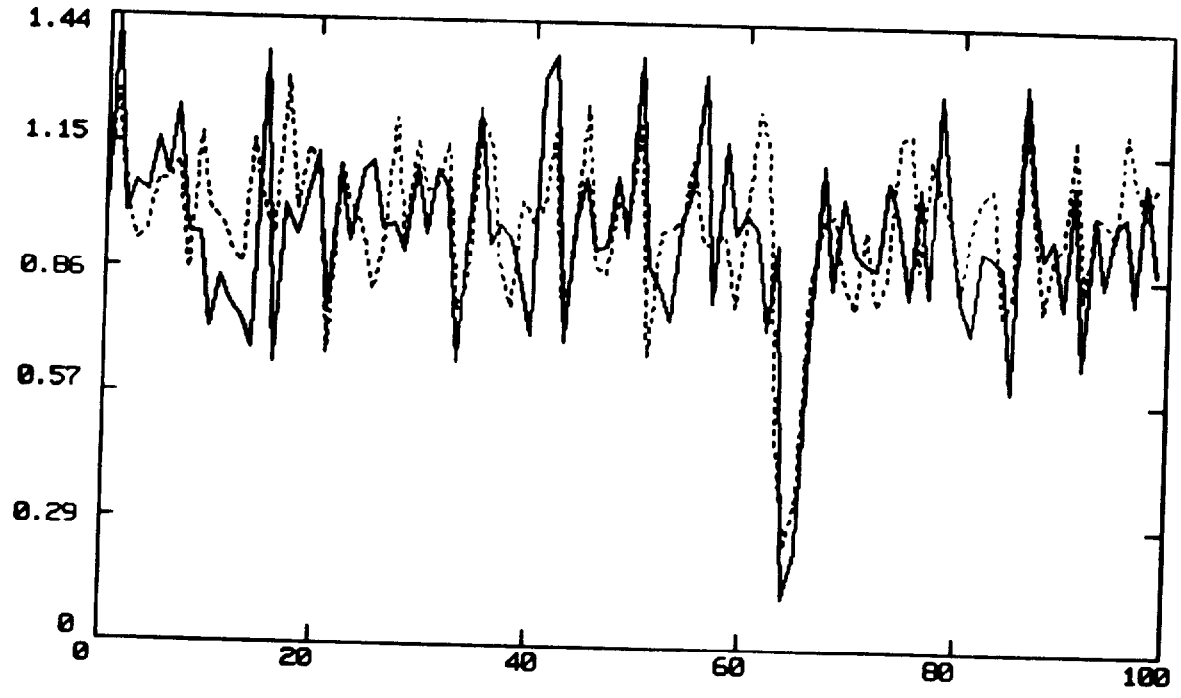


```
IUE_IDL>;column 150
IUE_IDL>;solid line: LWR 1233  dotted line: LWR 14533
```

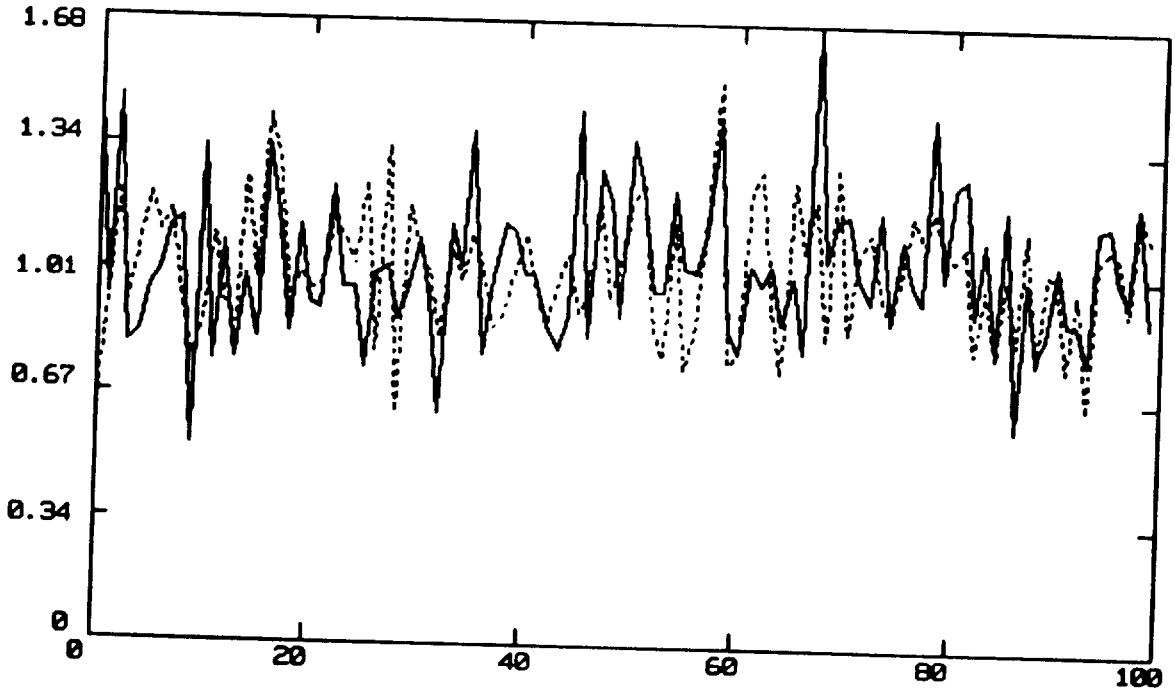

FIGURE 1

```
IUE_IDL>;line 150
IUE_IDL>;solid line: LWR 1233  dotted line: LWR 18067
```

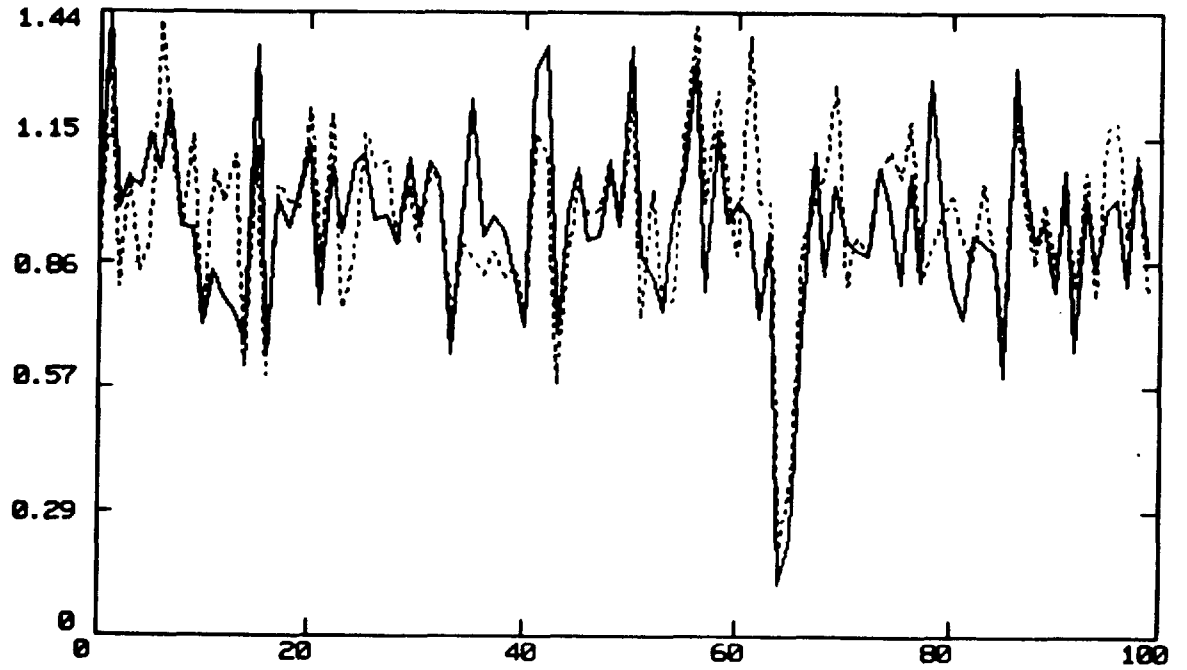


```
IUE_IDL>;column 150
IUE_IDL>;solid line: LWR 1233
IUE_IDL>;dotted line: LWR 18067
```

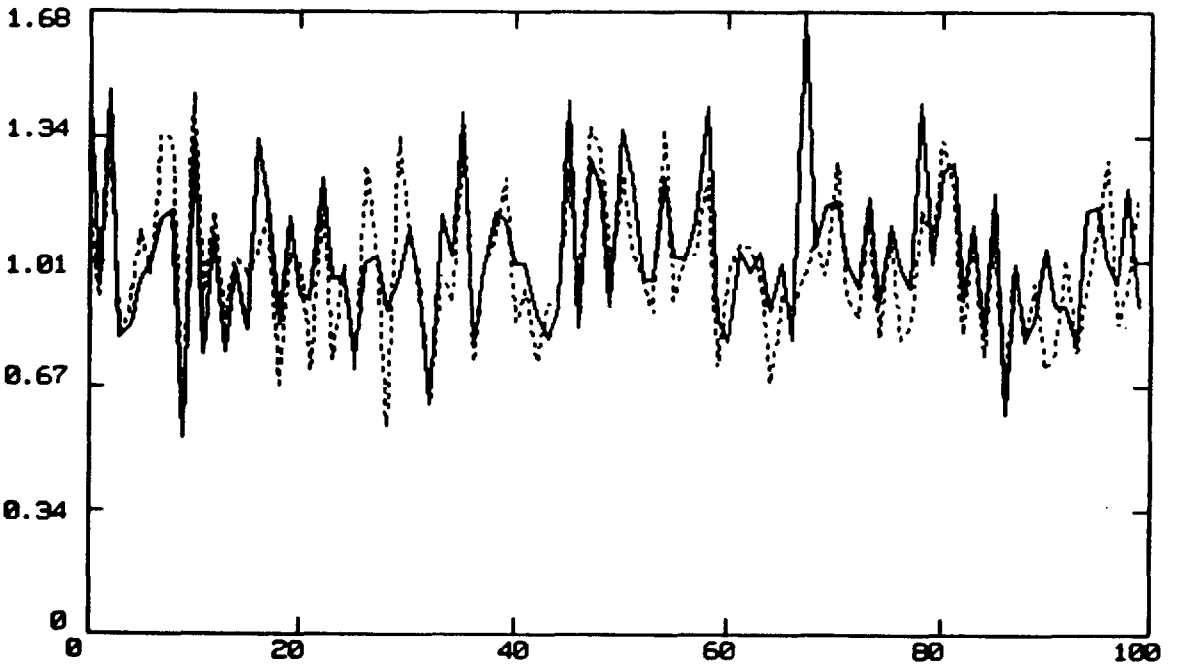

FIGURE 2

```
IUE_IDL>;line 150
IUE_IDL>;solid line: LWR 1230  dotted line:LWR 14535
```

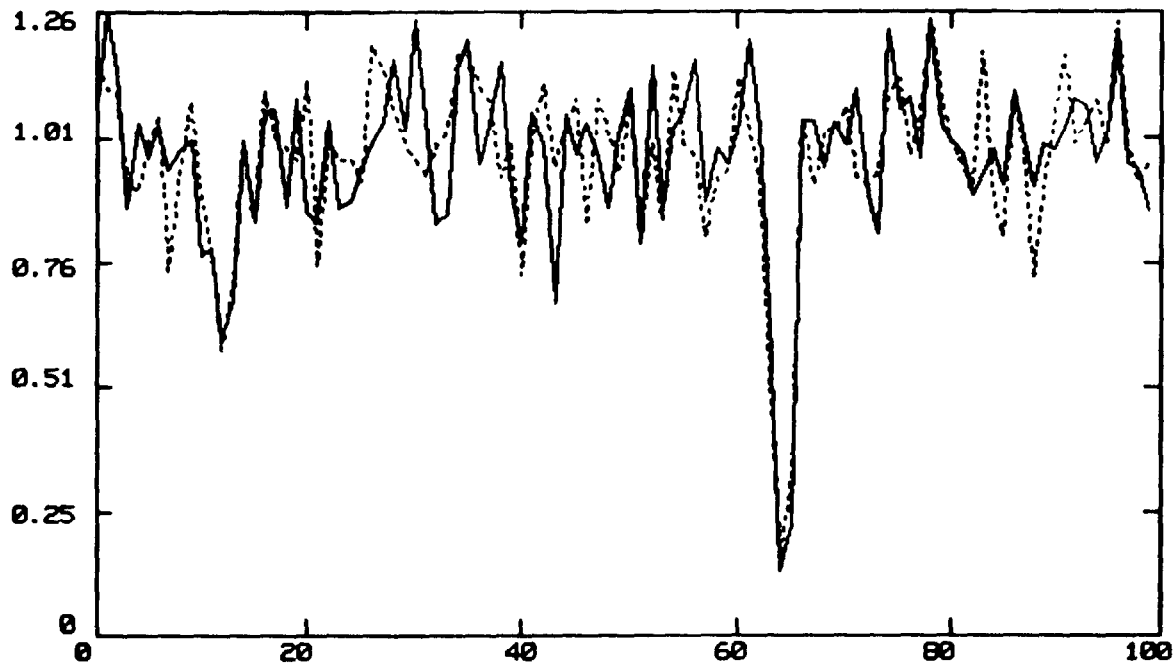


```
IUE_IDL>;column 150
IUE_IDL>;solid line: LWR 1230  dotted line: LWR 14535
```

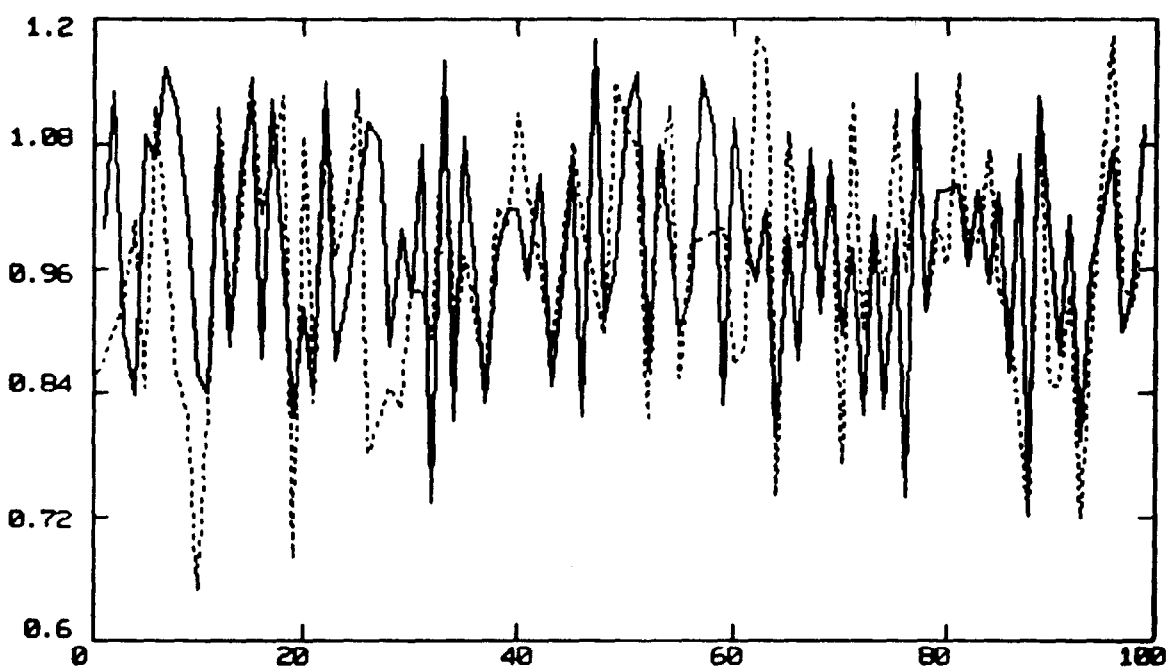

FIGURE 3

```
IUE_IDL>;line 150
IUE_IDL>;solid line: LWR 1230  dotted line: LWR 18069
```

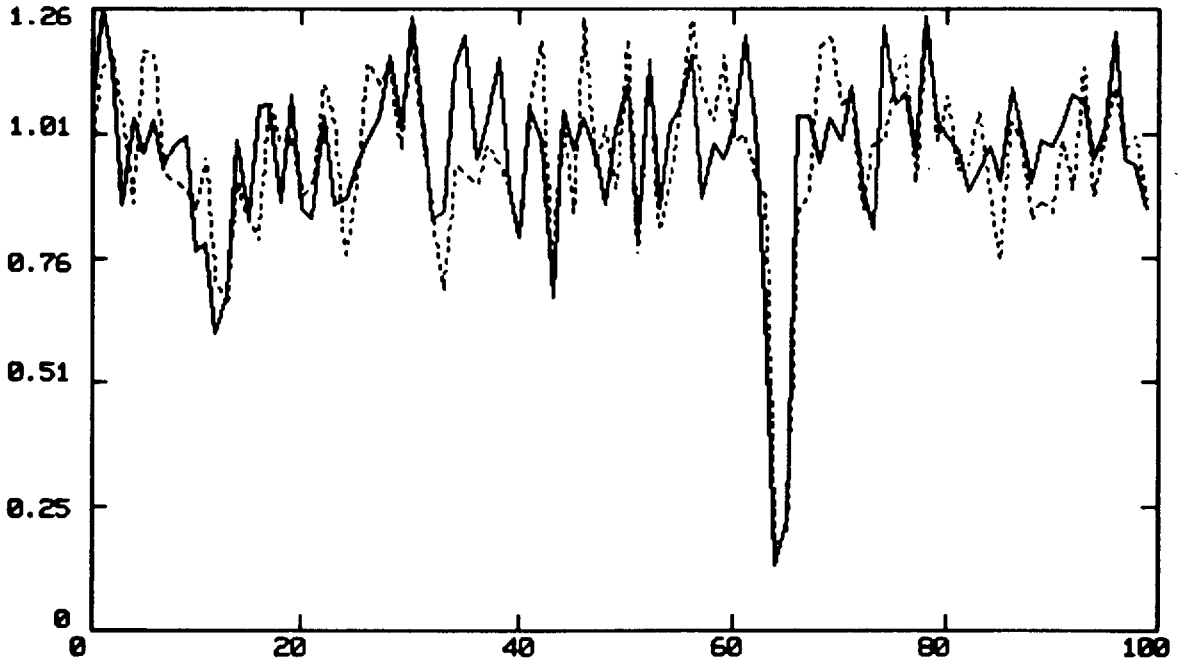


```
IUE_IDL>;column 150
IUE_IDL>;solid line: LWR 1230  dotted line: LWR 18069
```

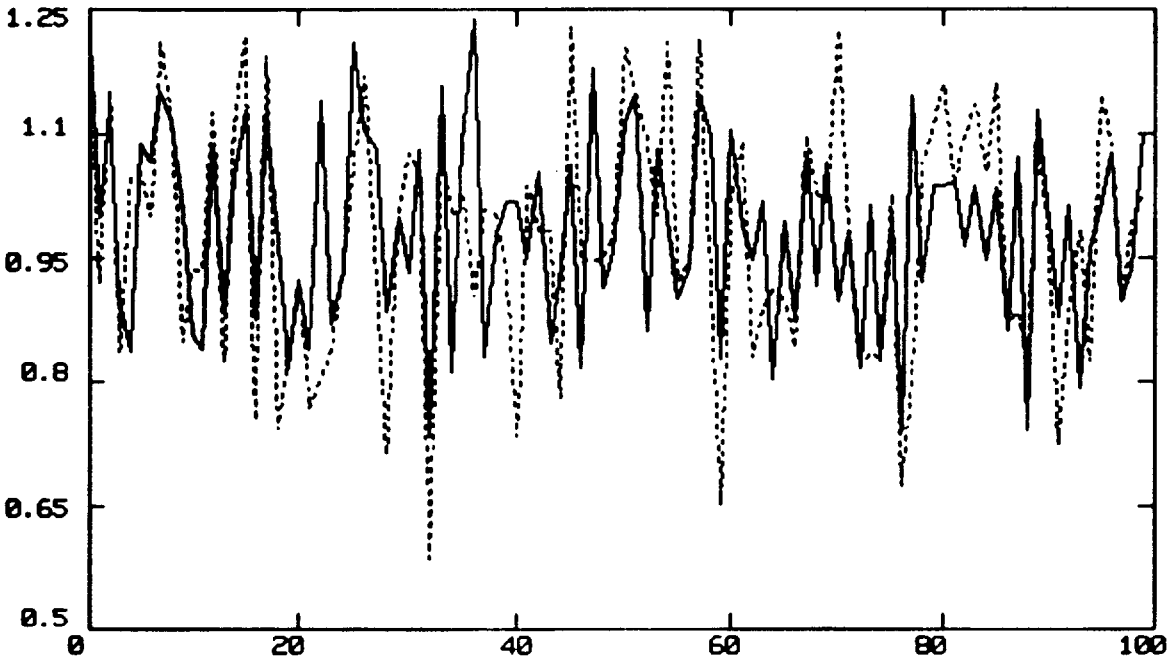

FIGURE 4

```
IUE_IDL>;line 150
IUE_IDL>;solid line:LWP 1468   dotted line: LWP 3431
```

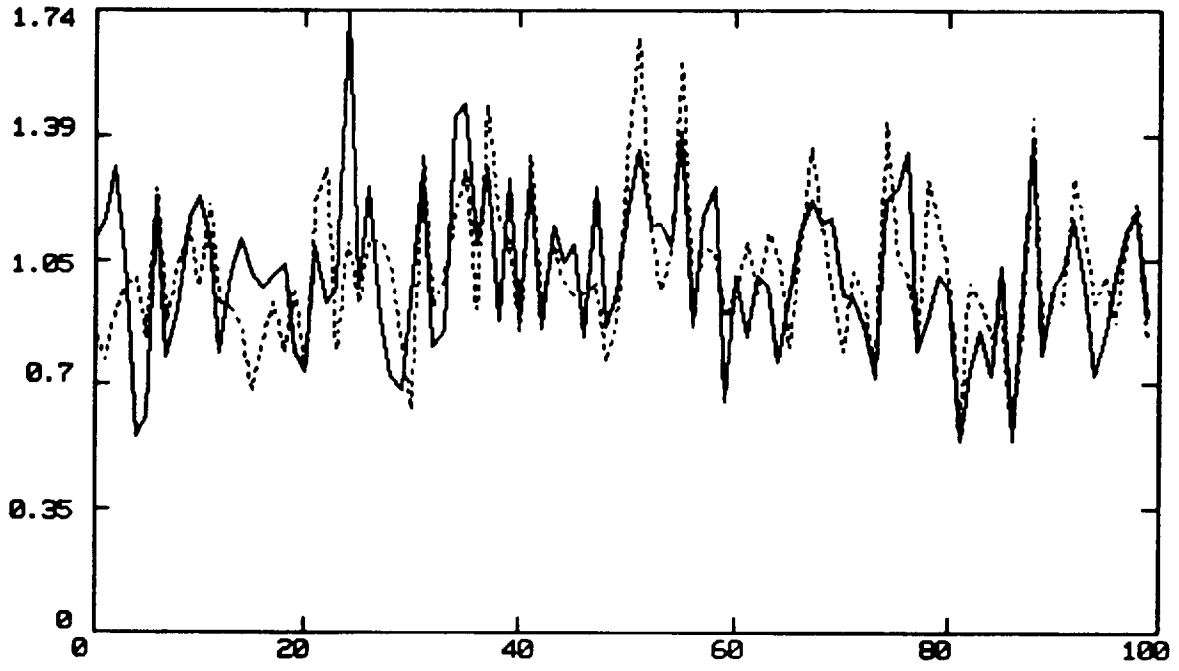


```
IUE_IDL>;column 150
IUE_IDL>;solid line:  LWP 1468    dotted line:   LWP 3431
```

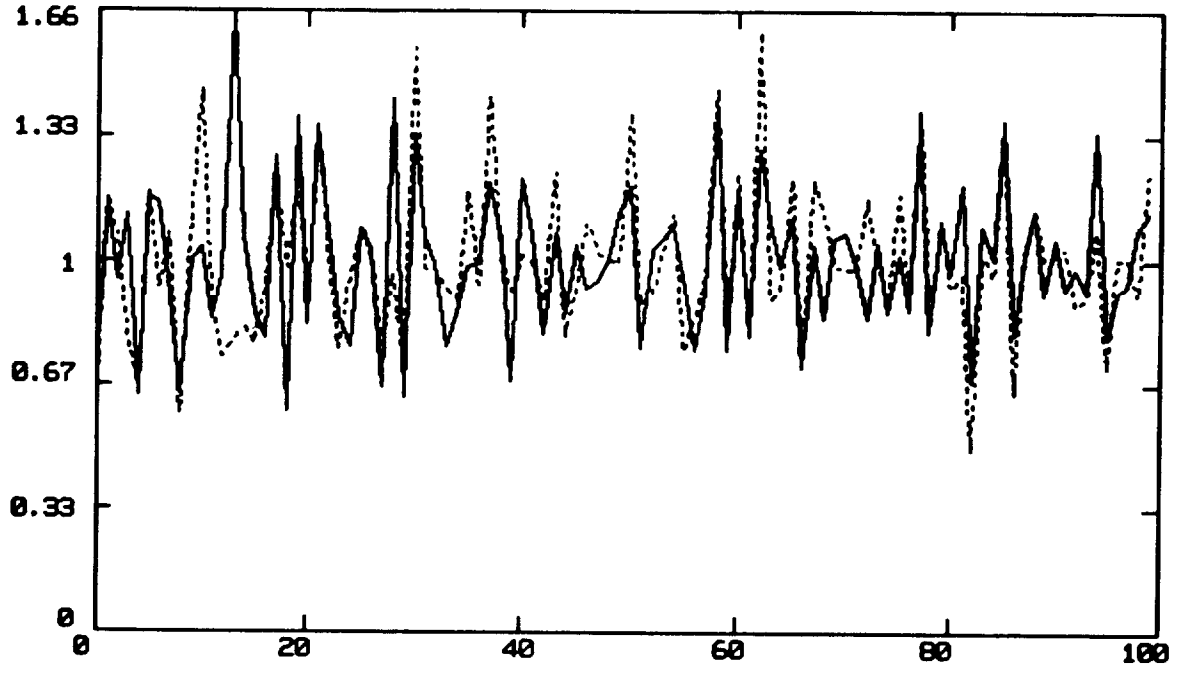

FIGURE 5

```
IUE_IDL>;line 150
IUE_IDL>;solid line: LWP 1470   dotted line  LWP 3433
```

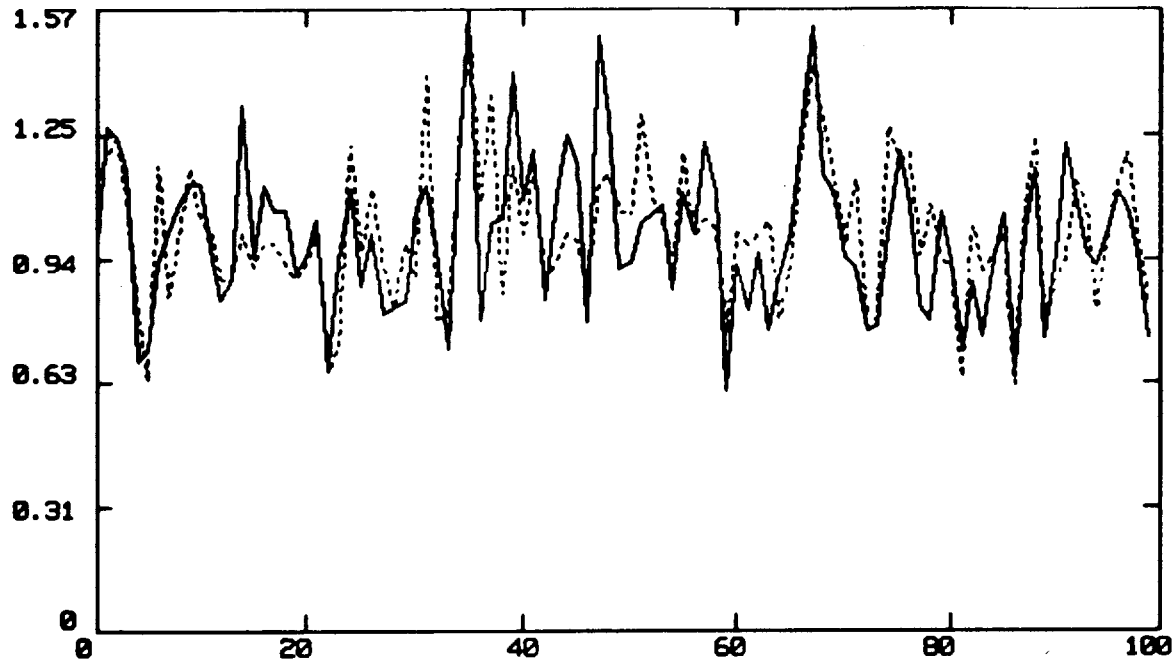

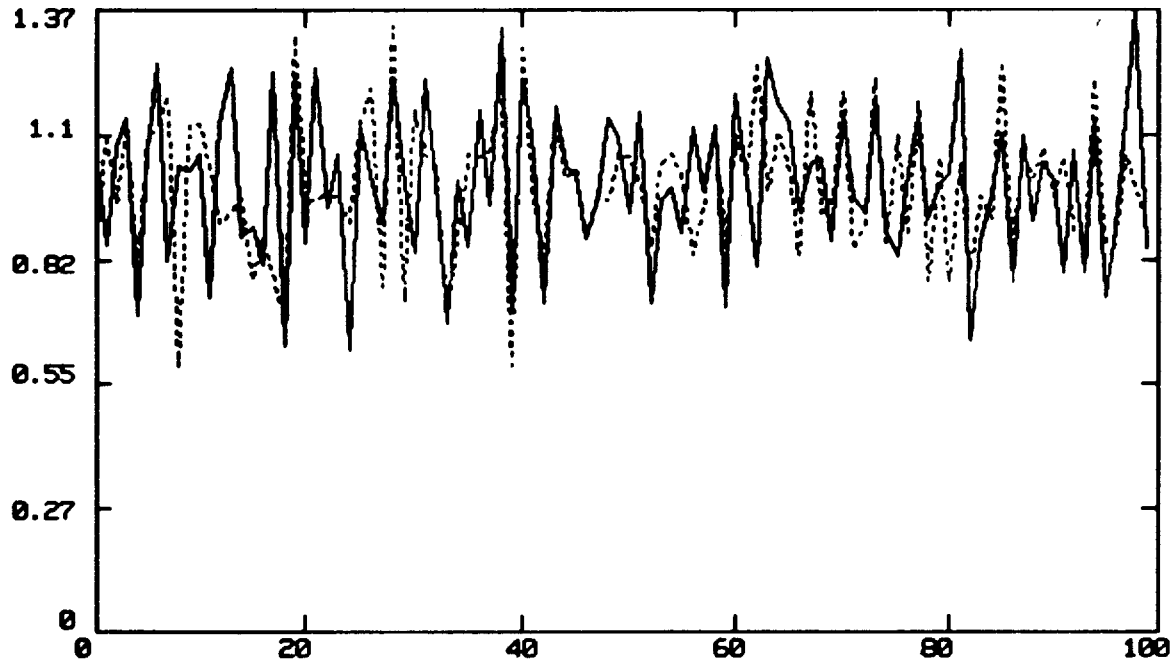

FIGURE 6

```
IUE_IDL>;line 150
IUE_IDL>;solid line: SWP 1252  dotted line: SWP 18591
```

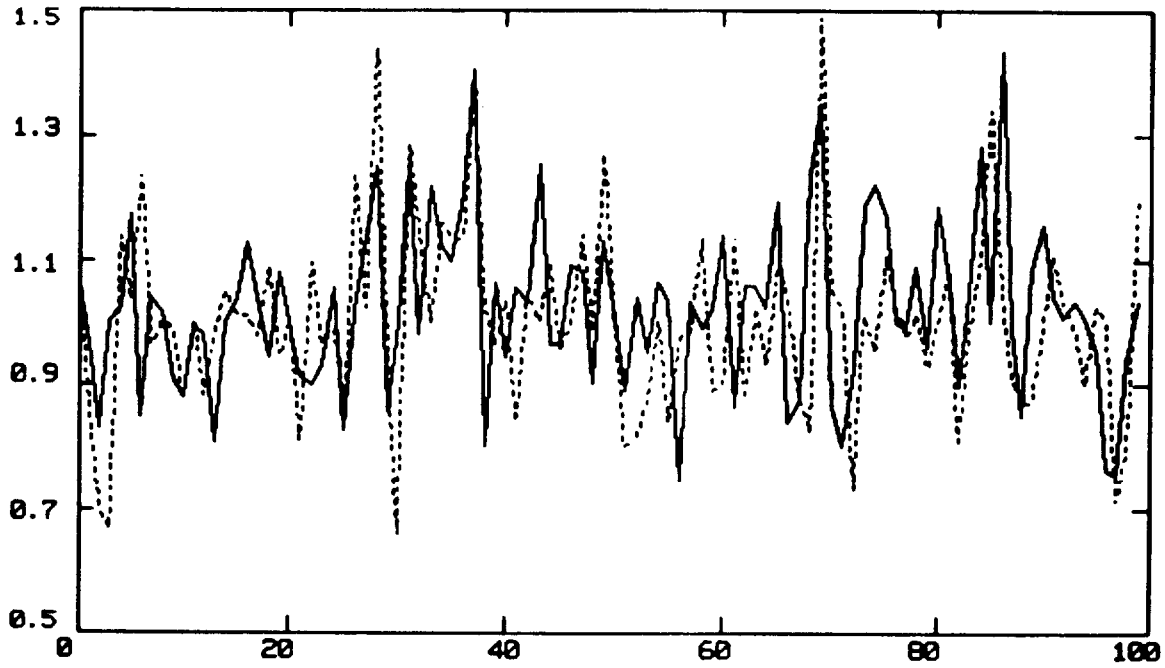


```
IUE_IDL>;column 150
IUE_IDL>;solid line: SWP 1252  dotted line: SWP 18591
```

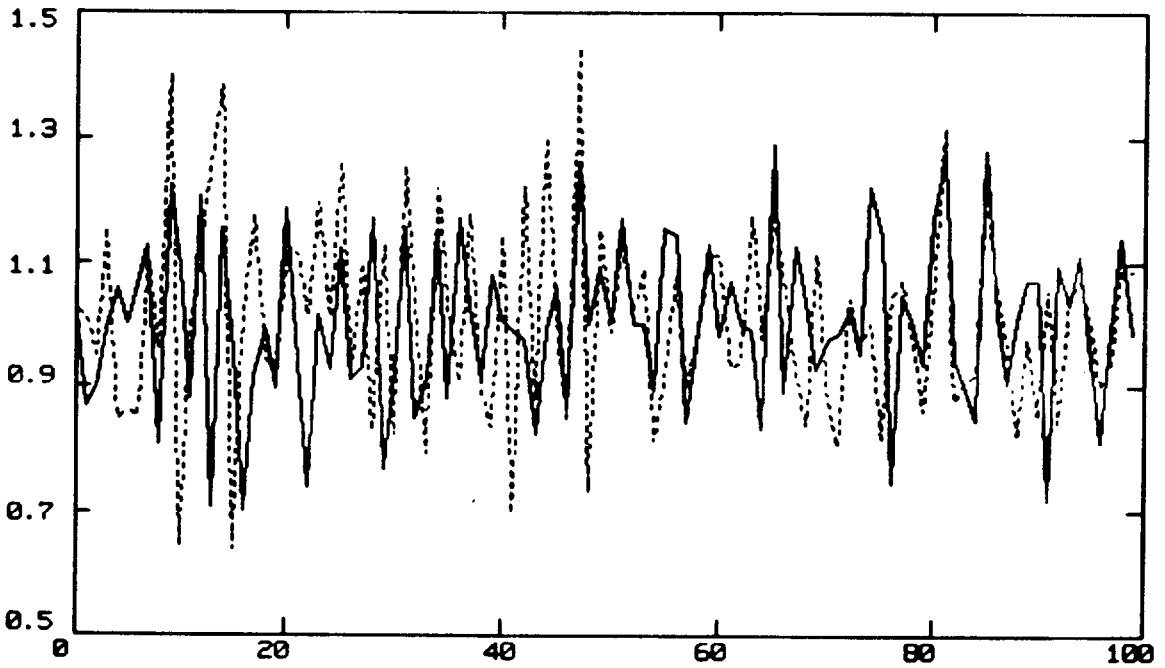

FIGURE 7

```
IUE_IDL>;line 150
IUE_IDL>;solid line: SWP 1252  dotted line: SWP 28016
```

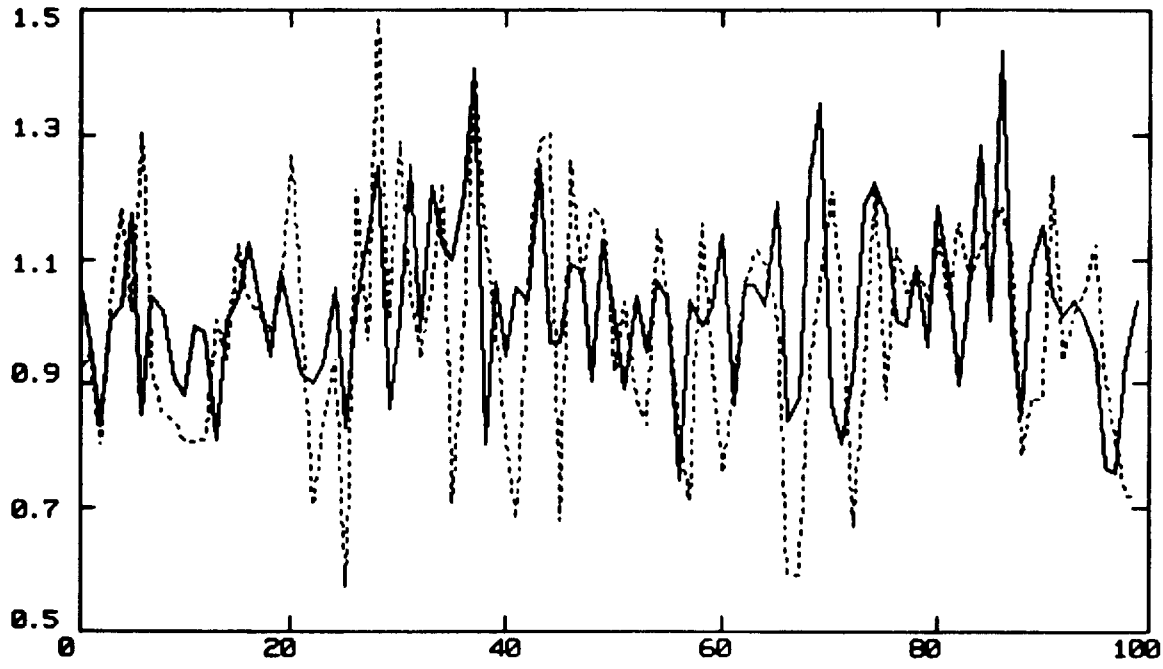


```
IUE_IDL>;column 150
IUE_IDL>;solid line: SWP 1252  dotted line: SWP 28016
```

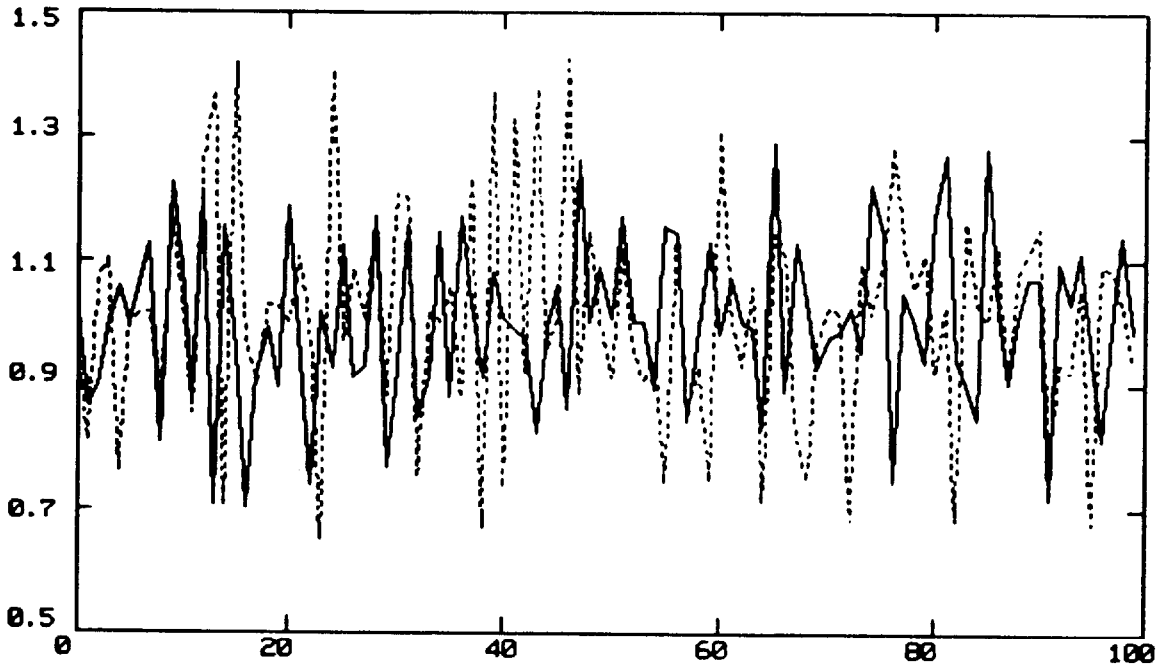

FIGURE 8

```
IUE_IDL>;line 150
IUE_IDL>;solid line: SWP 1243  dotted line: SWP 18590
```

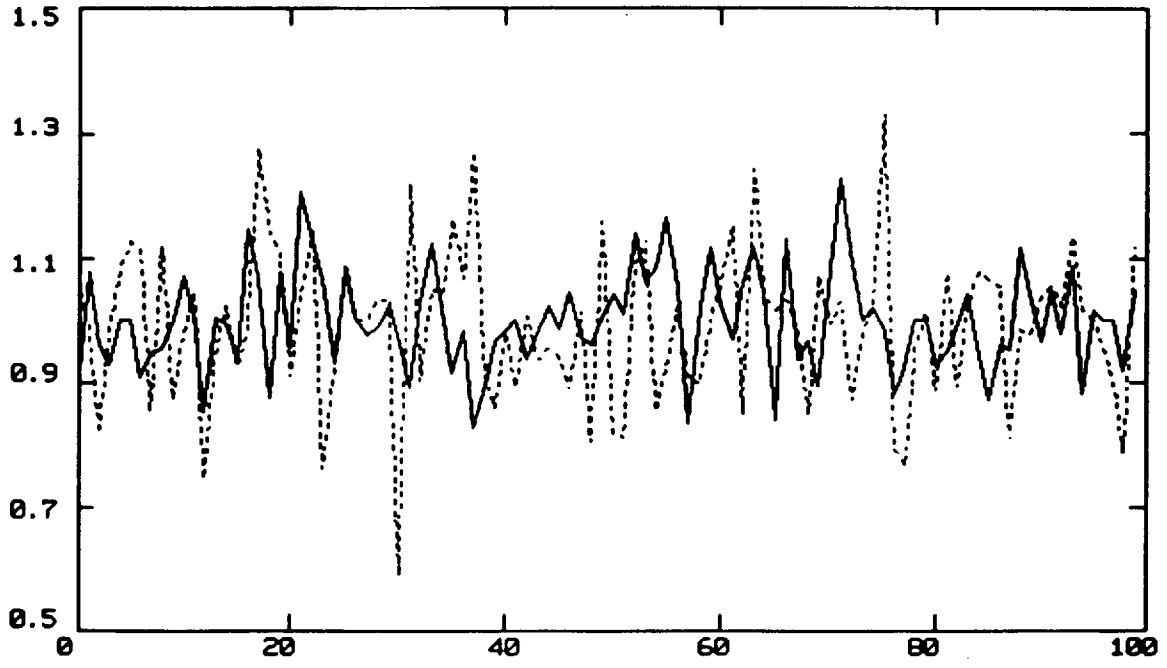


```
IUE_IDL>;column 150
IUE_IDL>;solid line: SWP 1243   dotted line: SWP 18590
```

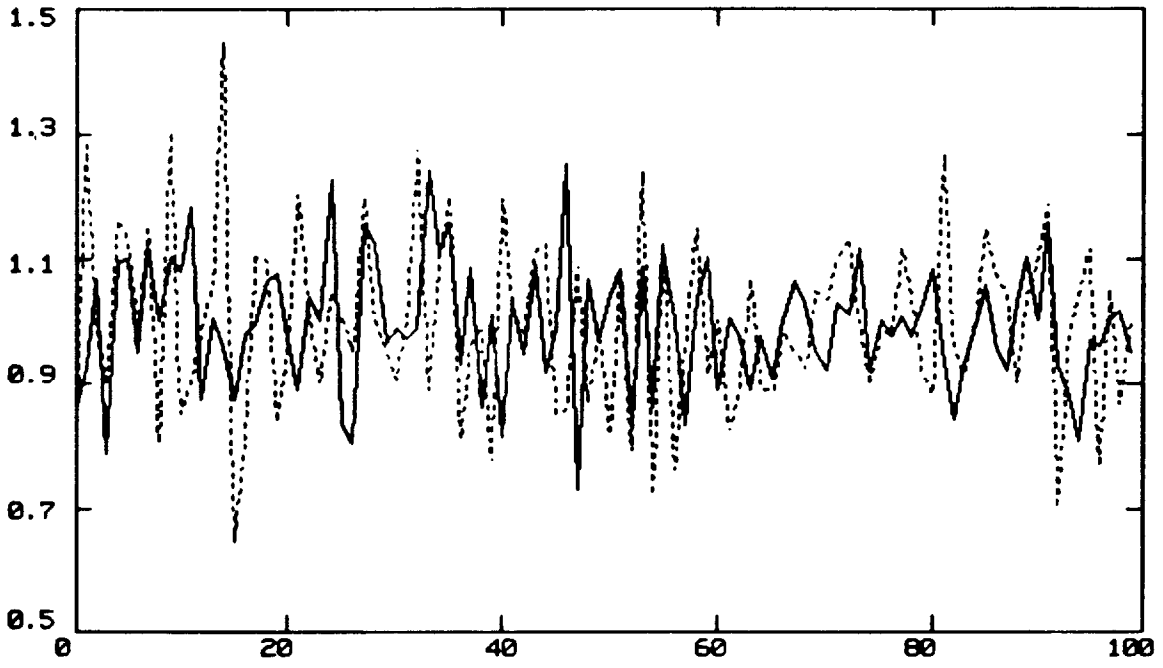

FIGURE 9

```
IUE_IDL>;line 150
IUE_IDL>;solid line: SWP 1243
IUE_IDL>;dotted line: SWP 28018
```

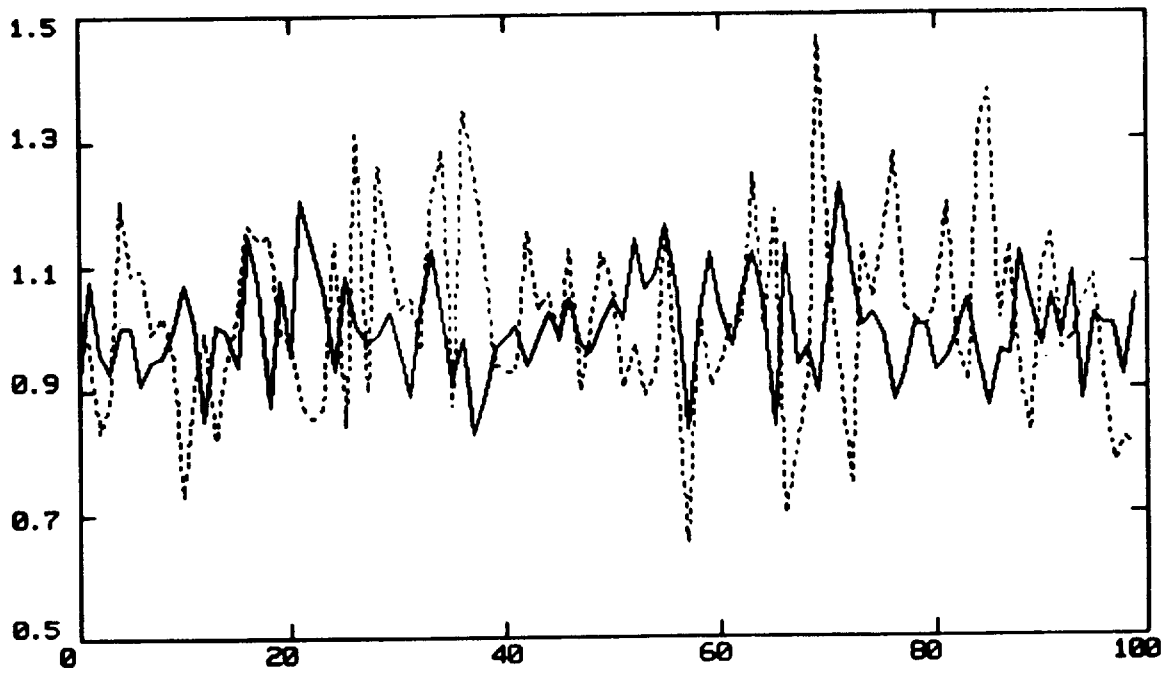


```
IUE_IDL>;column 150
IUE_IDL>;solid line: SWP 1243  dotted line: SWP 28018
```

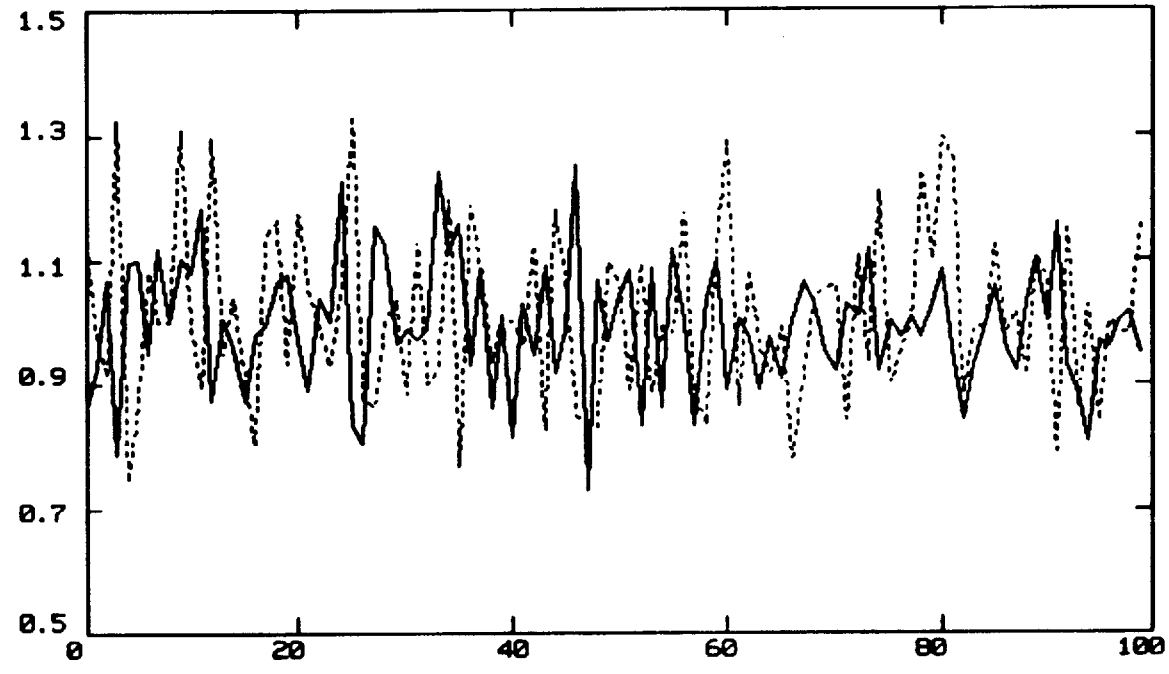

FIGURE 10

IUE_IDL>

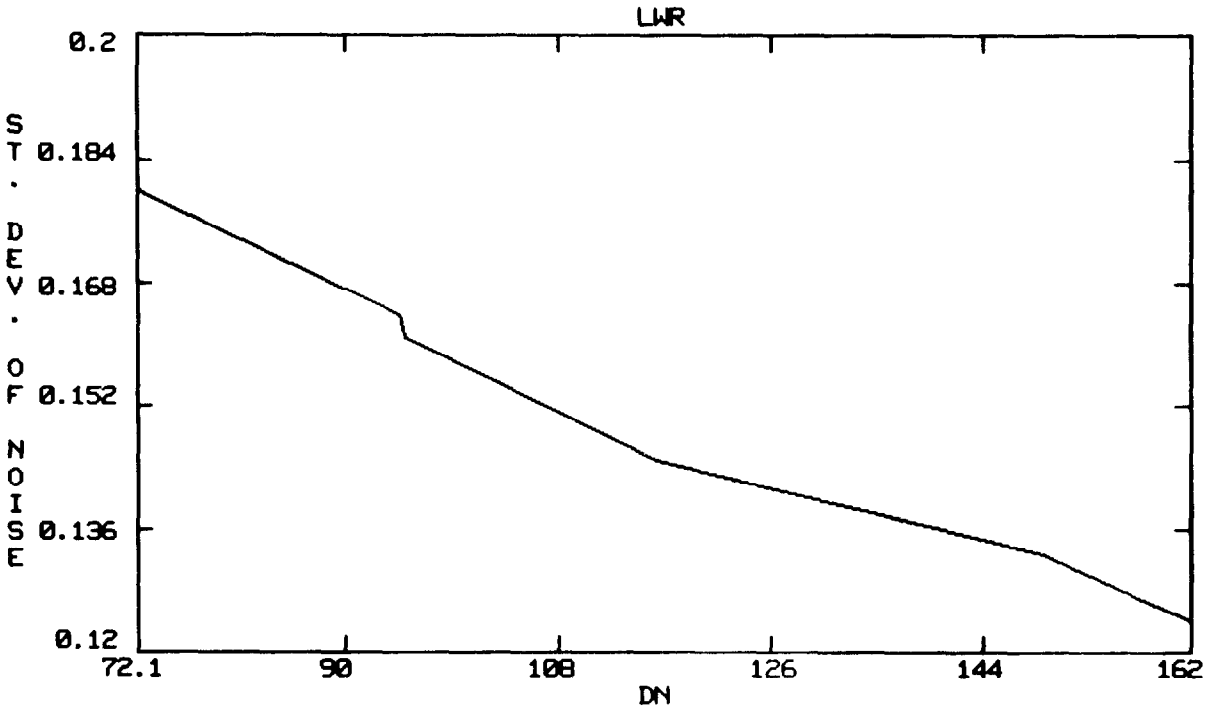

FIGURE 11

IUE_IDL>

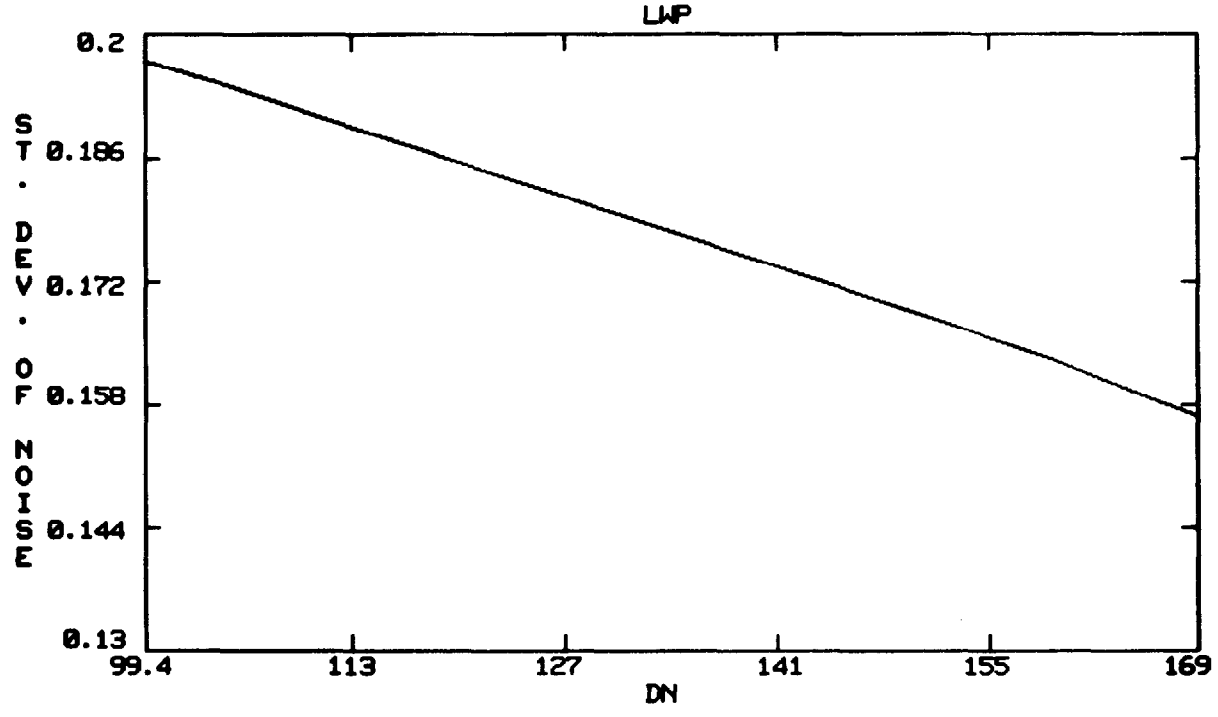

FIGURE 12

```
IUE_IDL>;average row
IUE_IDL>;solid line: SWP 1243  dotted line: SWP 28018
```

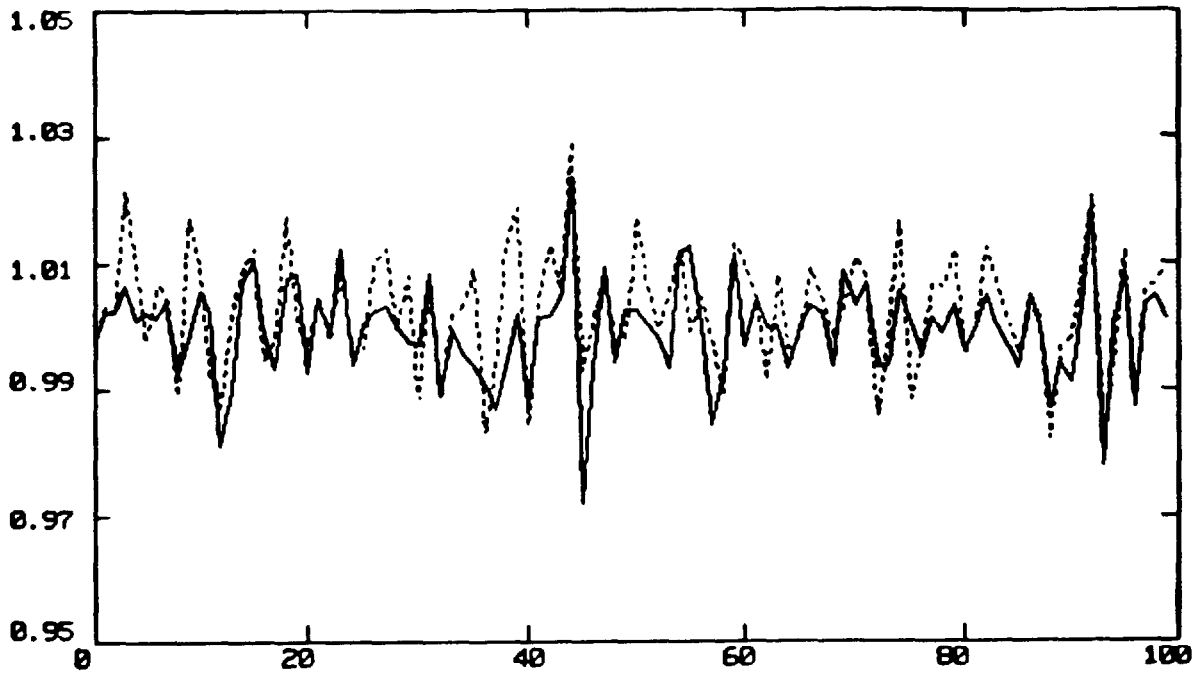

FIGURE 13

IUE_IDL>;FFT of average row LWP 1470

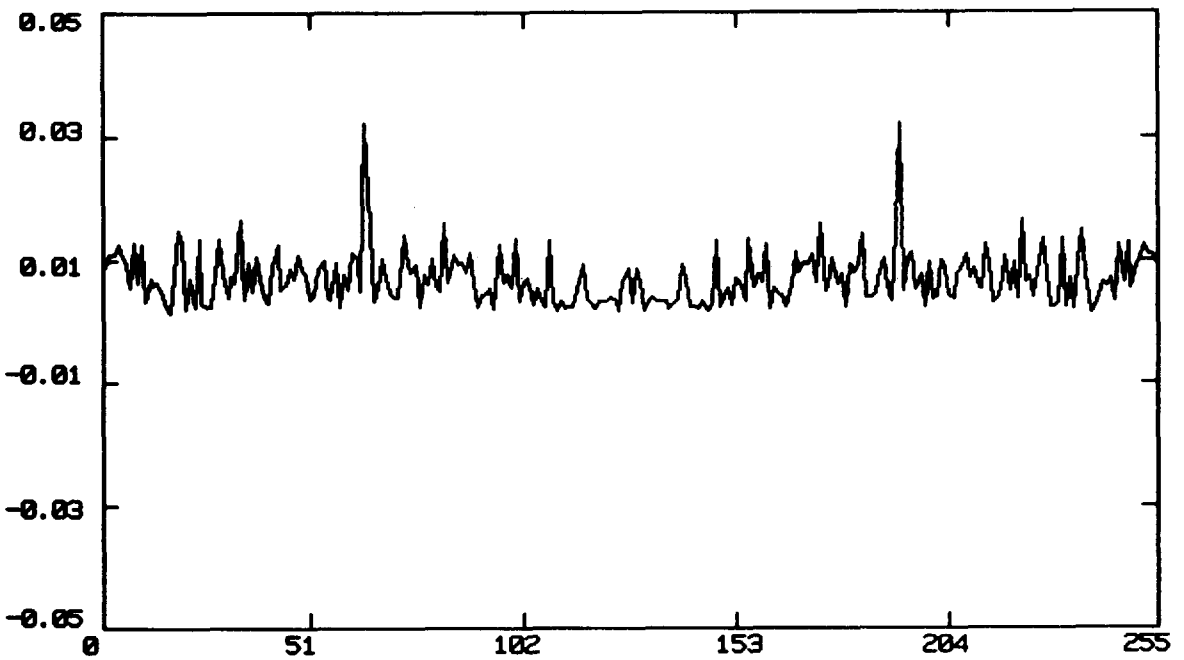

FIGURE 14

IUE_IDL>;FFT of average row SWP 1243

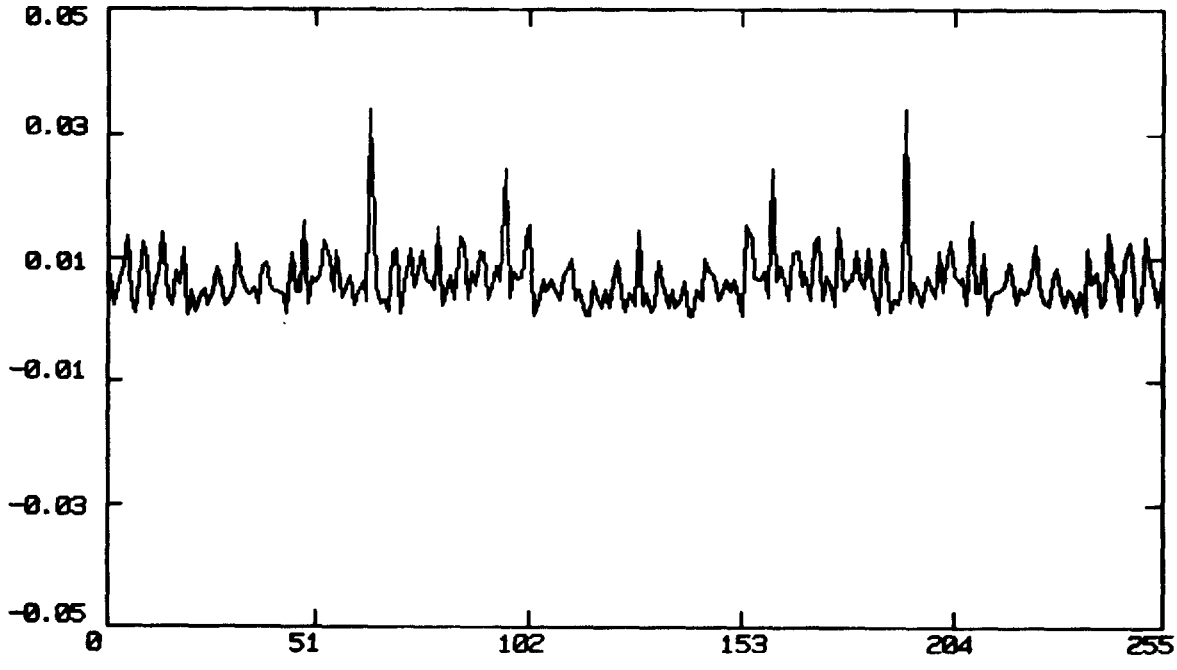

FIGURE 15

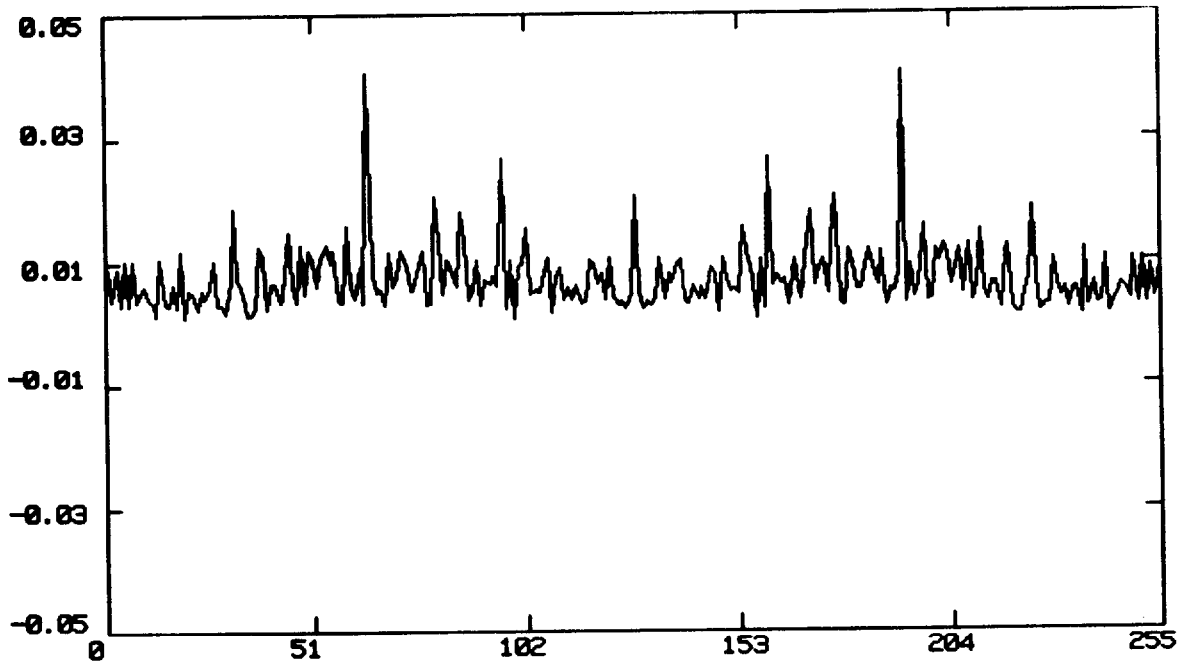
IUE_IDL>;FFT of average row SWP 28018
0.05
0.03
0.01
-0.01
-0.03
-0.05
0
51
102
153
204
255

FIGURE 16

IUE_IDL>;FFT of average row LWR 18069

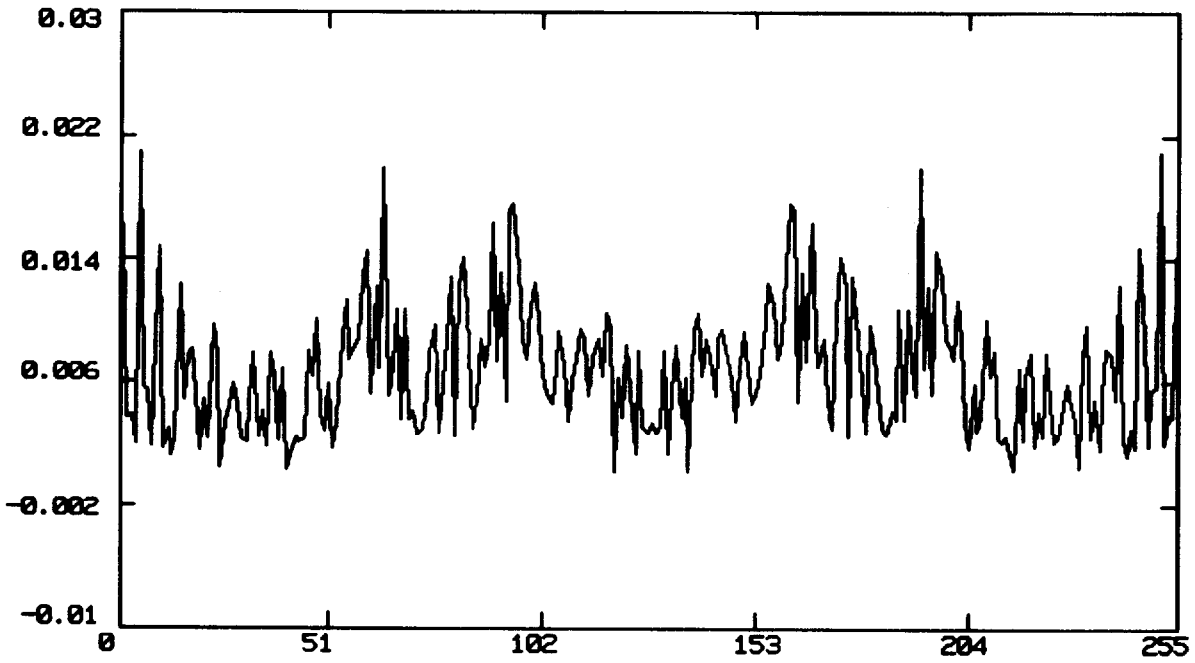

FIGURE 17

Appendix A

IUE SIGNAL-TO-NOISE RATIO ANALYSIS

References

"Investigation of Random and Fixed-Pattern Noise in High-Dispersion IUE Spectra", Adelman, S. and Leckrone, D., 1985, IUE Newsletter #28, 35.

"Improvement in Signal-to-Noise from Adding Low Dispersion Spectra", Clarke, J.T., 1981, IUE Newsletter #14, 149.

"Fixed Pattern Noise Revisited", Evans, N.R., 1987, preprint.

"Faint Object Studies with IUE", Gull, T.R., 1982, "Advances in Ultraviolet Astronomy", NASA CP-2238, 331.

"Improved Continuum Definition in High-Background IUE Images", Hackney, R.L., Hackney, K.R.H., and Kondo, Y., 1984, "Future of Ultraviolet Astronomy Based on Six Years of IUE Research", NASA CP-2349, 525.

"Spectral Anomalies in Low-Dispersion SWP Images", Hackney, R.L., Hackney, K.R.H., and Kondo, Y., 1982, "Advances in Ultraviolet Astronomy", NASA CP-2238, 335.

Joseph, C.L., 1984, Ph.D. Thesis, University of Colorado.

"A Medium Filter Subroutine", Schiffer, F.H. and Holm, A.V., 1980, IUE Newsletter #8, 41.

"The Interstellar Carbon Abundance. II. Rho Ophiuchi and Beta Scorpii", Welty, D.E., York, D.G., and Hobbs, L.M., 1986, Pub. Astron. Soc. of the Pac., 98, 857.

"A Study of the Reduction of Noise in IUE Spectra Obtained by Adding Extracted Spectra", West, K. and Shuttleworth, 1982, IUE Newsletter #19, 58.

"Observations of Interstellar Zinc", York, D.G. and Jura, M., 1982, Astrop. J., 254, 88.

"Spectra of Extragalactic Sources", York, D.G. et al., 1984, Astrophysical J., 276, 92.